



Geophysical Research Letters

Supporting Information for

Towards Hourly 4-D Subsurface Monitoring using Seismic Ambient Noise

Peng Guo^{1,*} and Erdinc Saygin^{1,2}

1. Deep Earth Imaging Future Science Platform, The Commonwealth Scientific and Industrial Research Organisation (CSIRO), Kensington 6151, WA, Australia.
2. Department of Physics, School of Physics, Mathematics and Computing, Faculty of Engineering and Mathematical Sciences, University of Western Australia, Crawley 6009, WA, Australia.

Corresponding author: Peng Guo (peng.guo@csiro.au)

Contents of this file

Text S1 – S2

Figures S1 to S16

Please note that, figures related to the Gorgon OBN survey are from Line 3924, unless otherwise stated.

Text S1.

Misfit function and adjoint source for trace-normalized FWI

The misfit function J for the trace-normalized FWI is defined as (Shen, 2010)

$$J = \sum_{i=1}^{N_s} \sum_{j=1}^{N_r} \left\| \frac{s_{i,j}}{\|s_{i,j}\|} - \frac{d_{i,j}}{\|d_{i,j}\|} \right\|^2 \quad (\text{S1}),$$

where $s_{i,j}$ and $d_{i,j}$ are seismic traces (1-D time-series vectors) from the synthetic and field data, respectively, i and j are the indexes for the sources and receivers, N_s and N_r are the number of sources and receivers, and $\| \cdot \|$ is the 1-2 norm operator.

Considering that $\frac{\partial \|s_{i,j}\|}{\partial s_{i,j}} = \frac{s_{i,j}}{\|s_{i,j}\|}$, the adjoint source is

$$\chi_{i,j} = \frac{\partial J}{\partial s_{i,j}} = \left(\frac{s_{i,j}}{\|s_{i,j}\|} - \frac{d_{i,j}}{\|d_{i,j}\|} \right) \left(\frac{\|s_{i,j}\| - \frac{s_{i,j}}{\|s_{i,j}\|} s_{i,j}}{\|s_{i,j}\|^2} \right) \quad (\text{S2})$$

Text S2.

Synthetic tests: sensitivity of time-lapse inversion to baseline model errors and data noise.

The observed temporal velocity changes (up to ~1%) is subtle, therefore it is important to test if these velocity changes are real, not coming from the unfitted data in the baseline inversion. We perform a series of synthetic tests. We use the same frequency range, recording geometry and inversion parameters of the field data for these tests. We use the FWI derived model (Fig. 4a) as the baseline model for generating the ‘observed’ baseline data. We then add 1% positive and negative Gaussian-shaped velocity anomalies (‘temporal changes’, 1 km horizontal extension and 0.2 km thickness, Fig. S11a) to the baseline model (Fig. 4a) for generating the ‘observed’ monitoring data. We first use the true baseline model (Fig. 4a) as the starting model for DD-WI as a benchmark, with the inverted models of velocity changes in Fig. S11b and S11c from DD-WI using waveform and travel time differences respectively.

The tomographic velocity model in Fig. S3a, which contains much larger difference with the true baseline model than the added velocity anomalies, is then used as the starting model for the DD-WI. By using the tomographic model as the baseline model, we create a scenario similar to the field data study where the differences between the baseline model used for inversion and the ground truth baseline model are very likely much larger than the observed temporal changes, and we are able to test the robustness of time-lapse inversion to baseline models. Both the DD-WI methods using waveform (Yang et al., 2016) and travel time differences have been applied. The results suggest that the proposed algorithm is able to recover the subtle velocity differences very well (Fig. S12c), and is less sensitive to the baseline model than DD-WI using waveform differences (Fig. S12b). We then add noise to the baseline and monitoring data respectively. The signal to noise ratio (S/N) is ~ 8 , lower than that of the extracted hourly CC functions, and the inverted models (Fig. S13) suggest that DD-WI using travel times is more robust to noise. Fig. S14 suggests that the method is able to recover more subtle velocity perturbations (0.5%).

We also test if the inversion methods and data settings can recover velocity anomalies of smaller size (0.5 km horizontal extension and 0.2 km thickness, Fig. S15a). When using the true baseline model (Fig. 4a) as the starting model for time-lapse inversion (which is not going to happen in field data studies, benchmark test), DD-WI using waveform differences can recover the anomalies better (Fig. S15). However, when there are errors in the baseline model, DD-WI using travel time differences provides better results (Fig. S16). Therefore the proposed method is robust to data noise and errors in the baseline model, and the velocity temporal changes localized by DD-WI using travel time differences are reliable.

Gorgon OBN Seismic Survey (2015-2016)

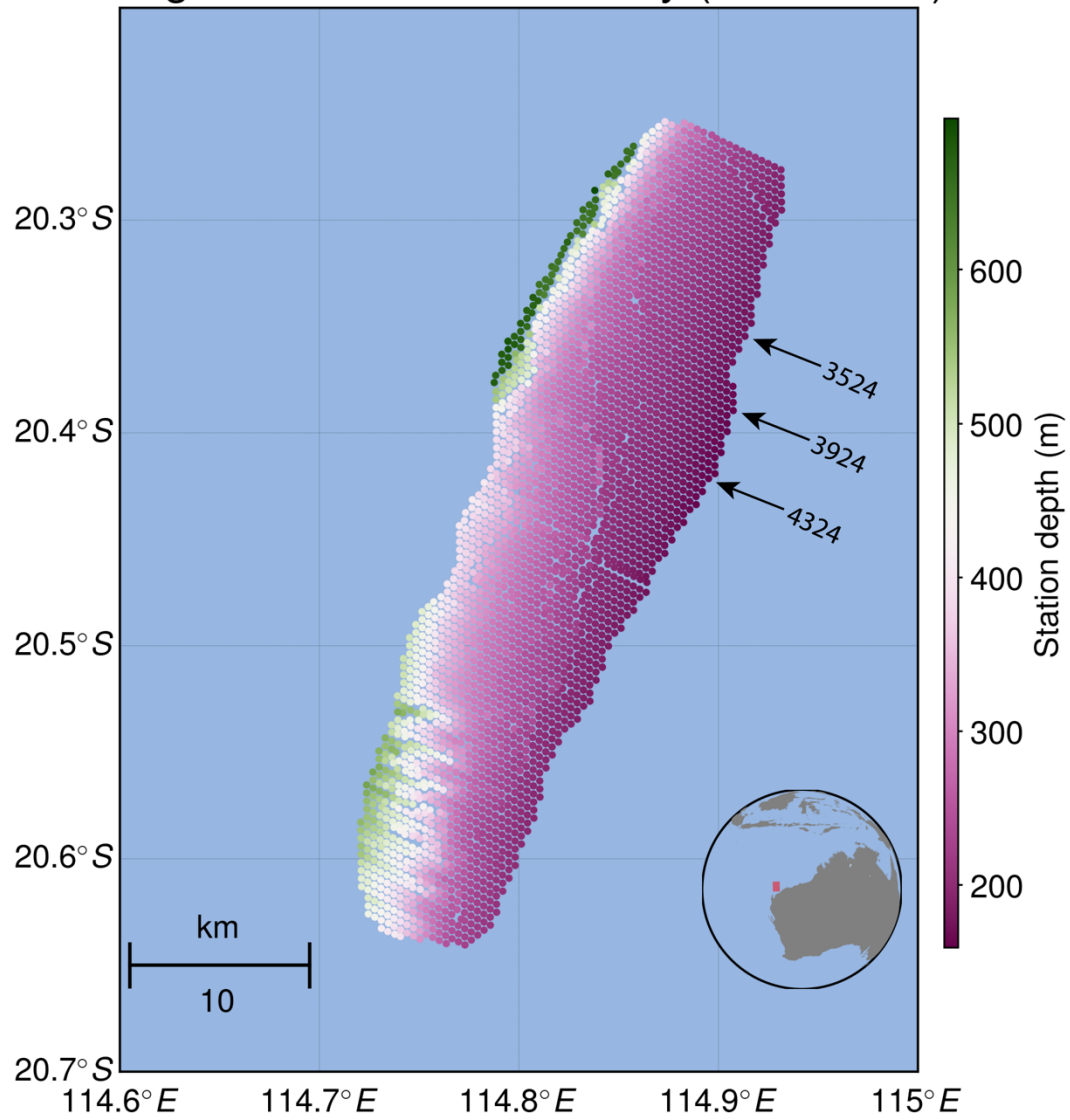


Figure S1. Ocean Bottom Node (OBN) seismic survey in the Gorgon gas field of the offshore of Western Australia by Chevron Australia and its partners. The colors on the OBNs suggest water depths. The black arrows indicate the positions of Line 3524, 3924 and 4324, respectively.

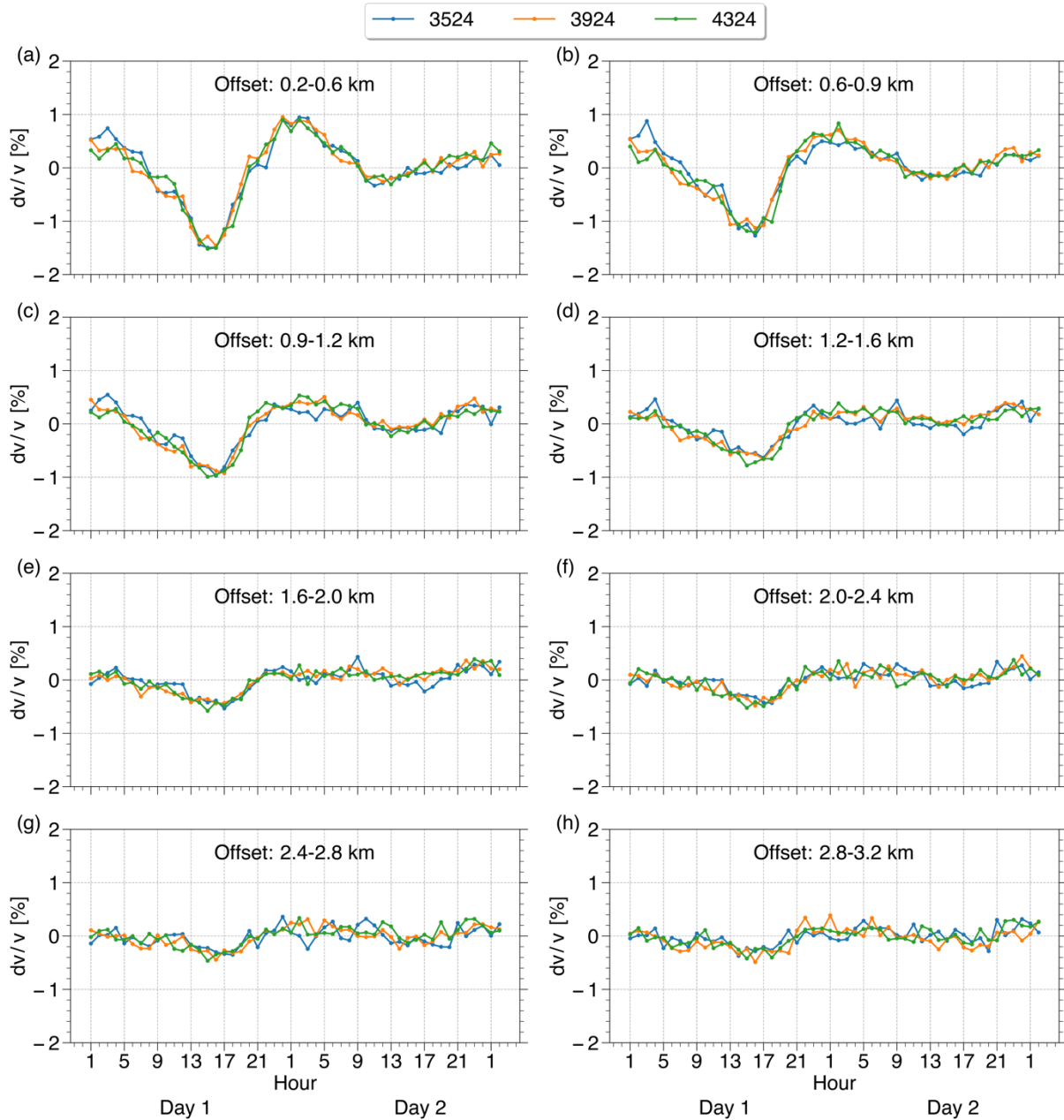


Figure S2. The shear-wave velocity changes (dv/v) of the seafloor at an hourly basis for Day 1 and Day 2 of 2016 from Lines 3524, 3924 and 4324, from CC functions of different offset ranges. The velocity changes were estimated using the stretching method from the ballistic part of the extracted Scholte waves of the CC functions.

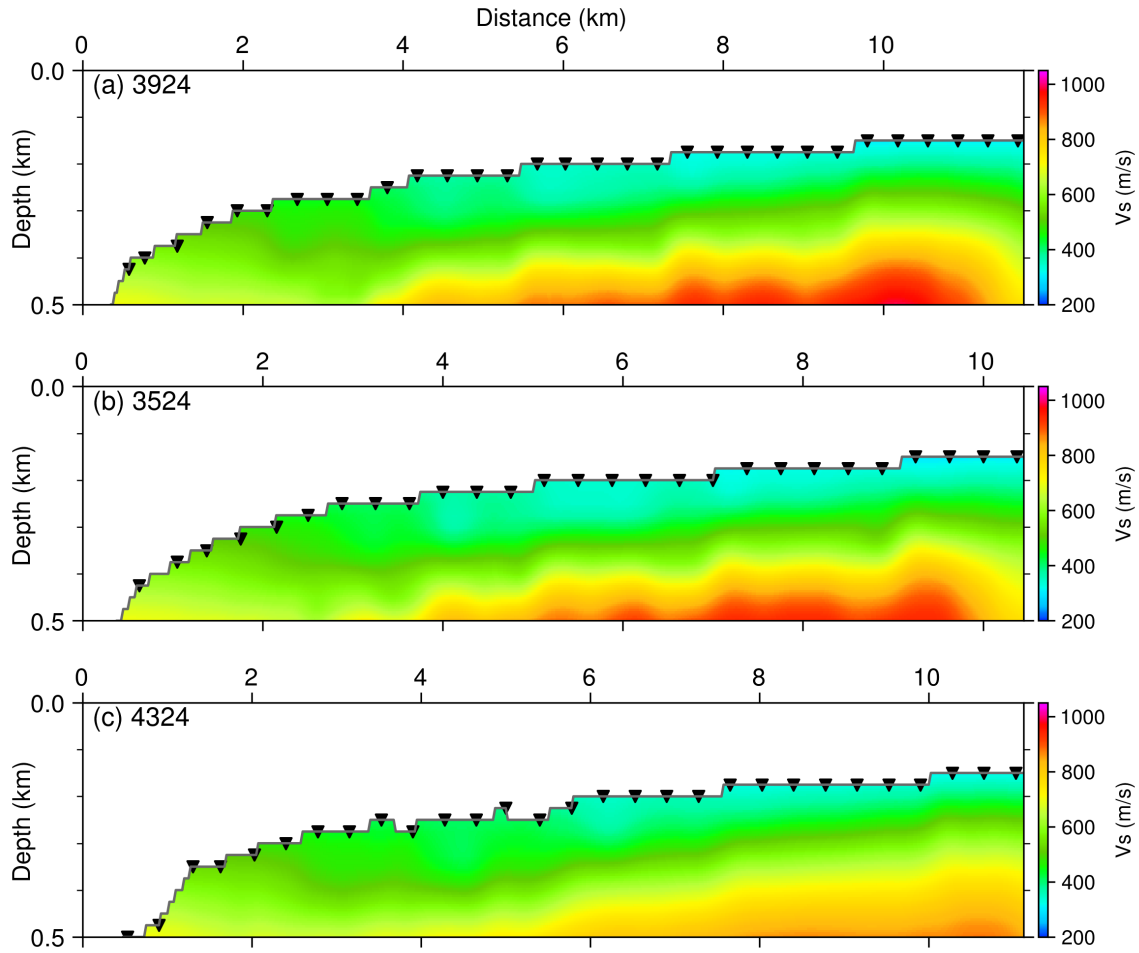


Figure S3. The velocity models from wave-equation dispersion inversion (Chen & Saygin, 2022), which are used as the starting models for baseline FWI. (a), (b) and (c) are the shear-wave velocity models for Line 3924, 3524 and 4324 (Fig. S2), respectively.

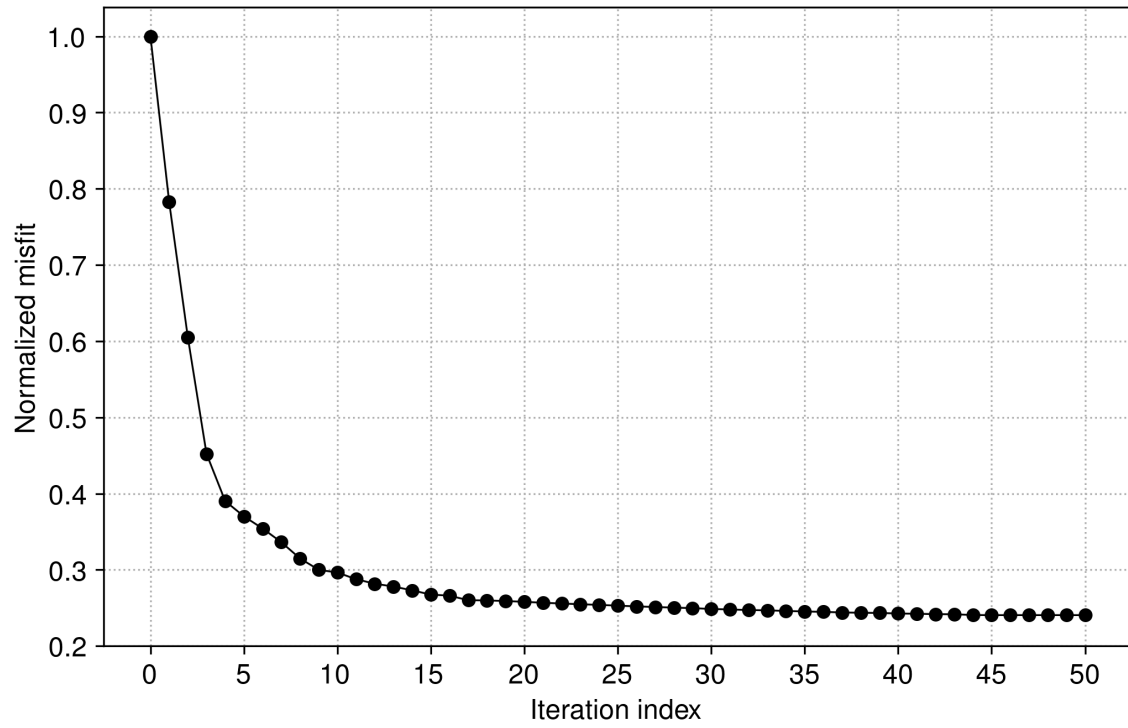


Figure S4. Waveform misfit as a function of iterations for trace-normalized FWI (baseline FWI). The waveform misfit was calculated using equation S1.

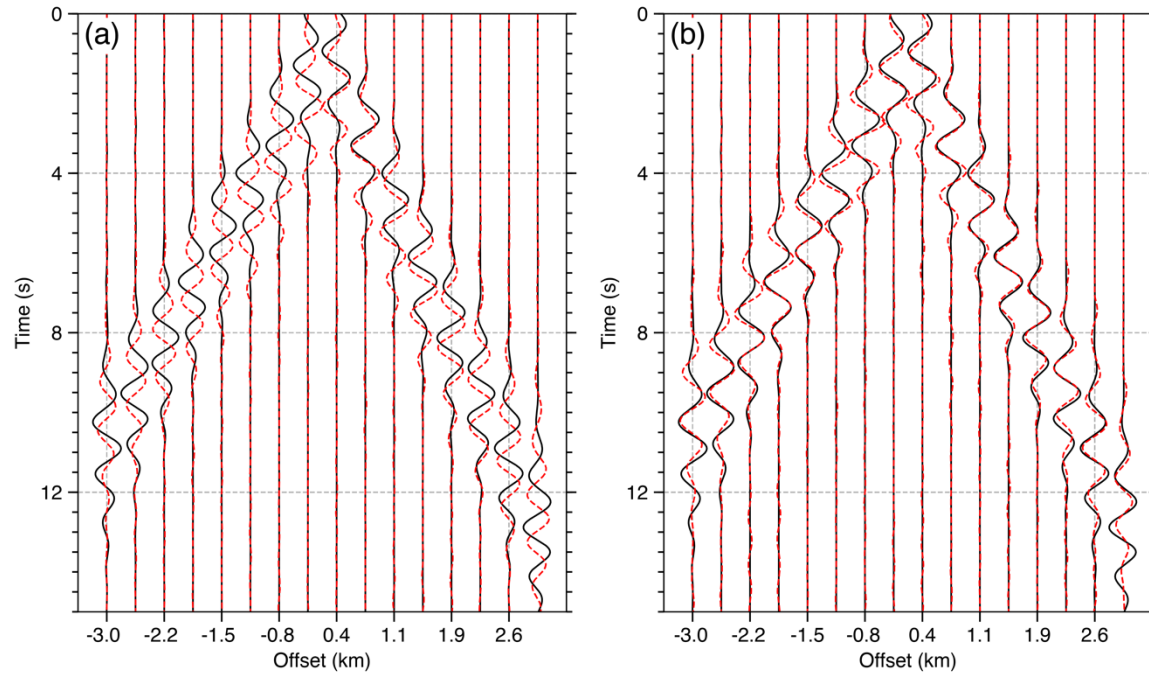


Figure S5. A comparison of observed (extracted from ambient noise) and synthetic seismic waveform data. (a) The observed data (black) and the synthetic waveform (dashed red) using the starting model (Fig. S3a) of baseline FWI, and (b) the observed data (black) and the synthetic waveform (dashed red) using the final model from baseline FWI (Fig. 4a). The waveform match between observed and synthetic data has been much improved after baseline FWI.

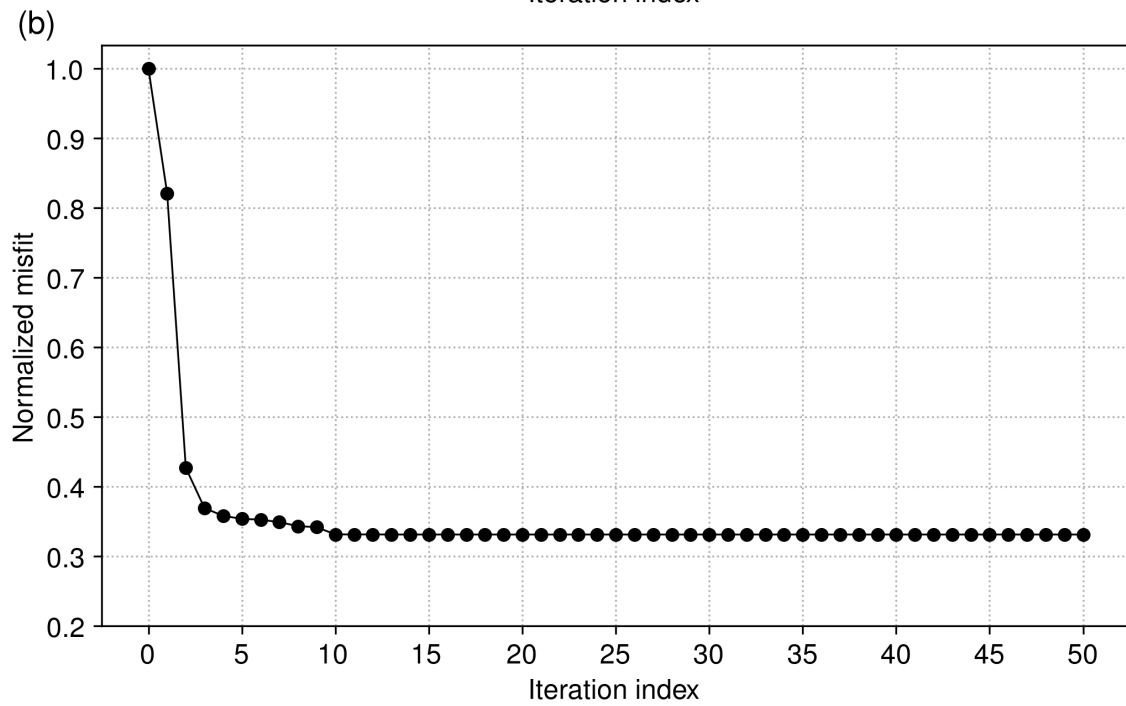
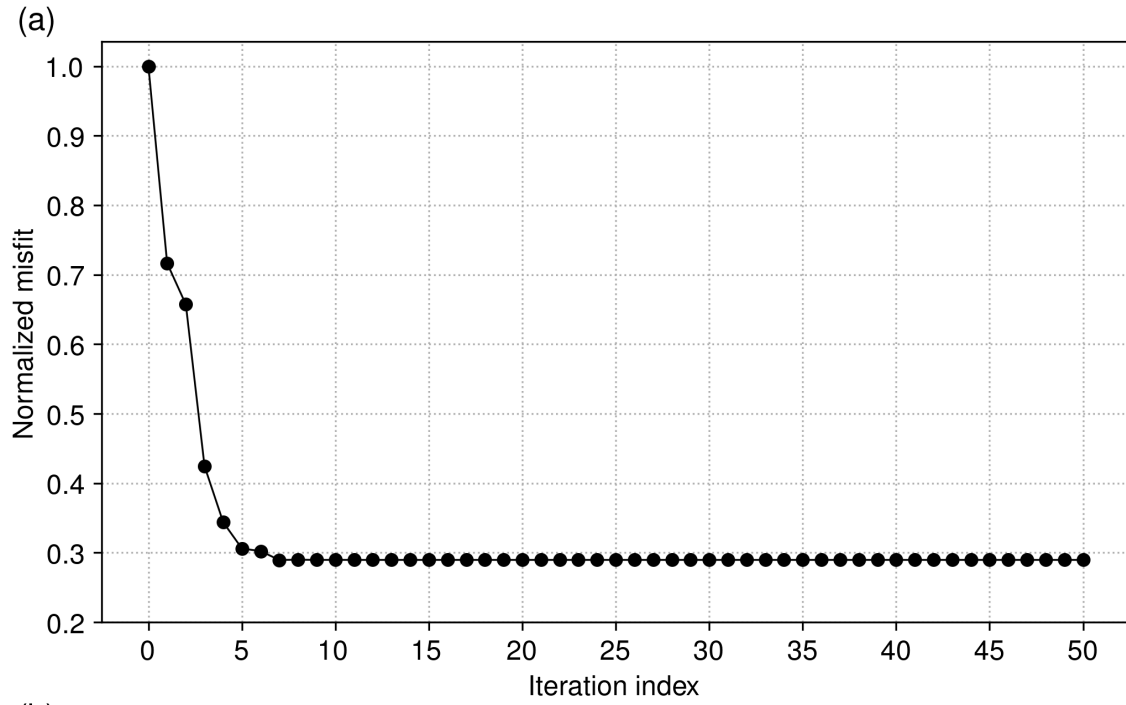


Figure S6. Misfit as a function of iterations for DD-WI, for (a) Hour 15 Day 1 and (b) Hour 1 Day 2. The misfit was calculated using equation 1.

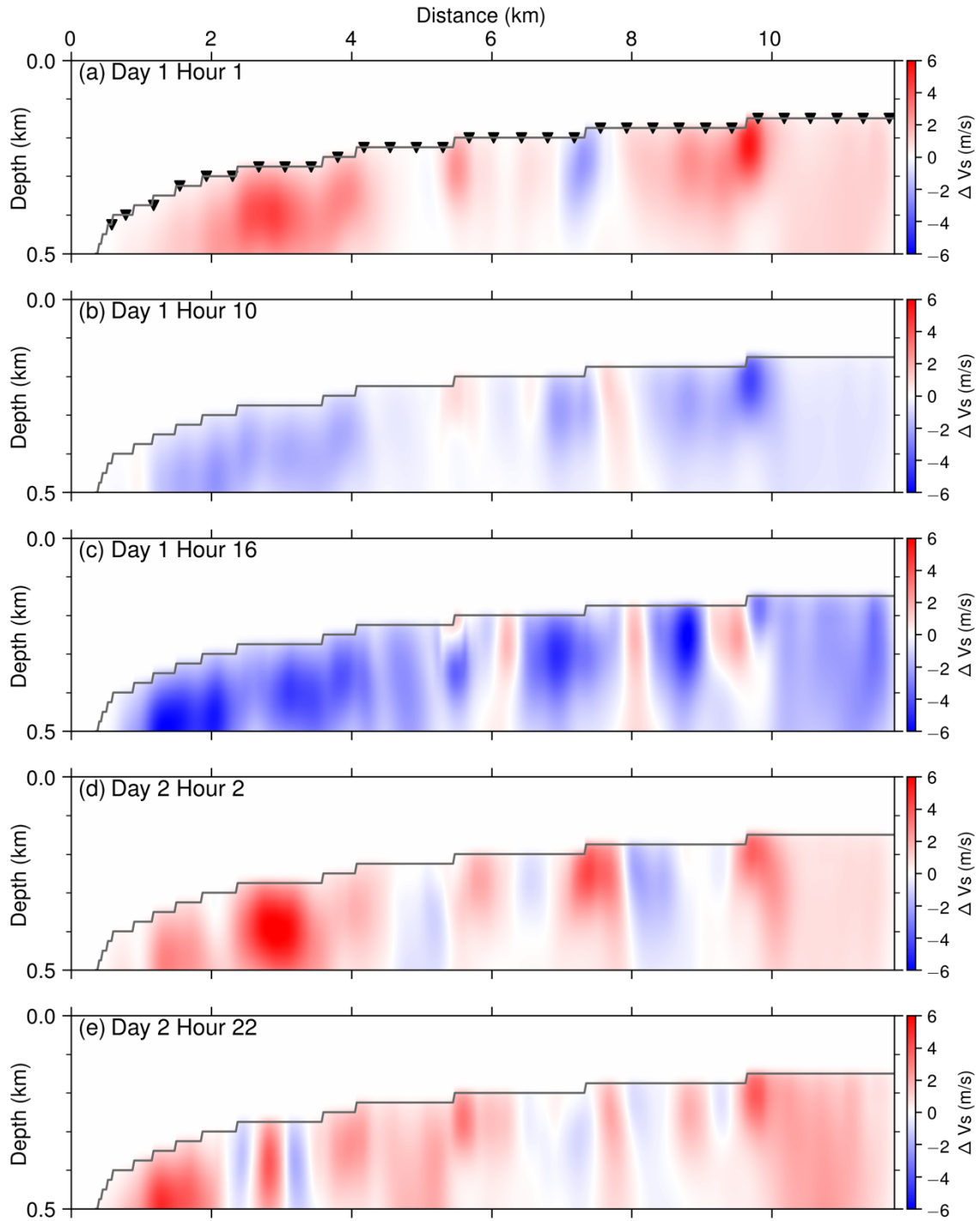


Figure S7. Time-lapse subsurface models of velocity changes from more hours compared with the baseline model (Fig. 4a). The black triangles in (a) indicate the locations of OBNs.

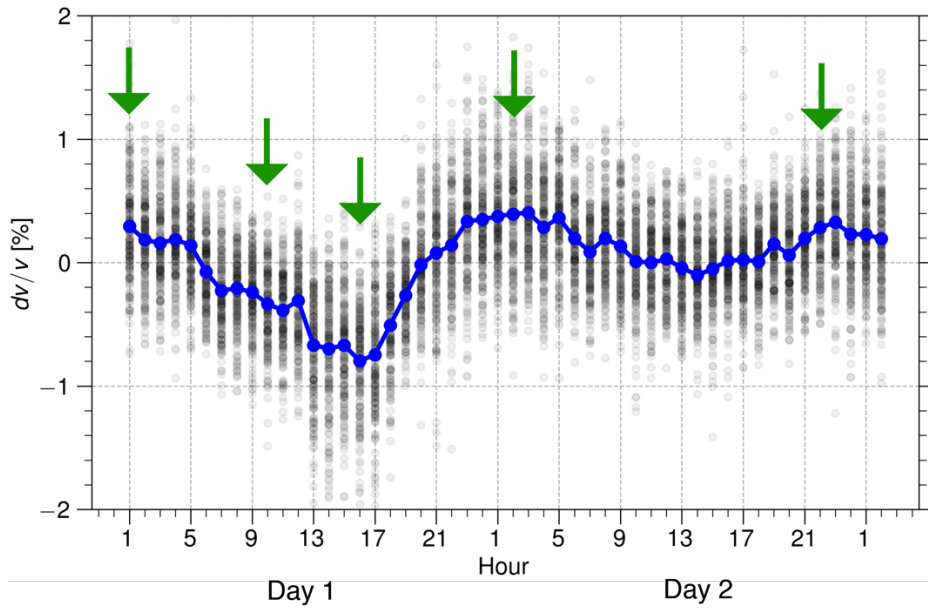


Figure S8. The relative shear-wave velocity changes (dv/v) of the seafloor at an hourly basis for Day 1 and Day 2 of 2016 (the same with Fig. 2a), estimated using the stretch method assuming a spatially homogeneous dv/v . The green arrows from left to right indicate the dv/v for the time-lapse images in Fig. S7 from top to bottom.

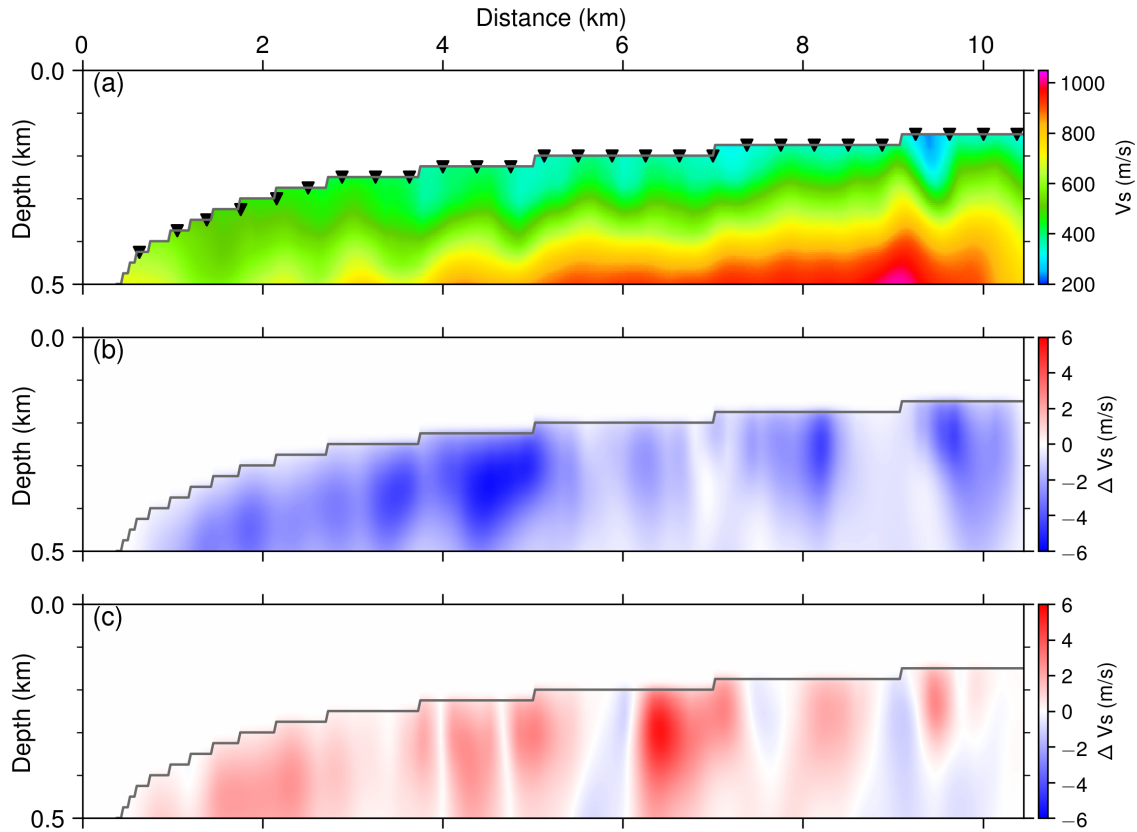


Figure S9. Baseline velocity model and time-lapse subsurface models of velocity changes in the shallow seafloor for Line 3524. The starting model for baseline FWI is Fig. S3b. (a) The high-resolution baseline velocity model from trace-normalized FWI, which is used as the starting model for DD-WI. (b) The time-lapse image of velocity changes for Hour 15 Day 1. (c) The time-lapse image of velocity changes for Hour 1 Day 2. The black triangles in (a) indicate the locations of the OBNs.

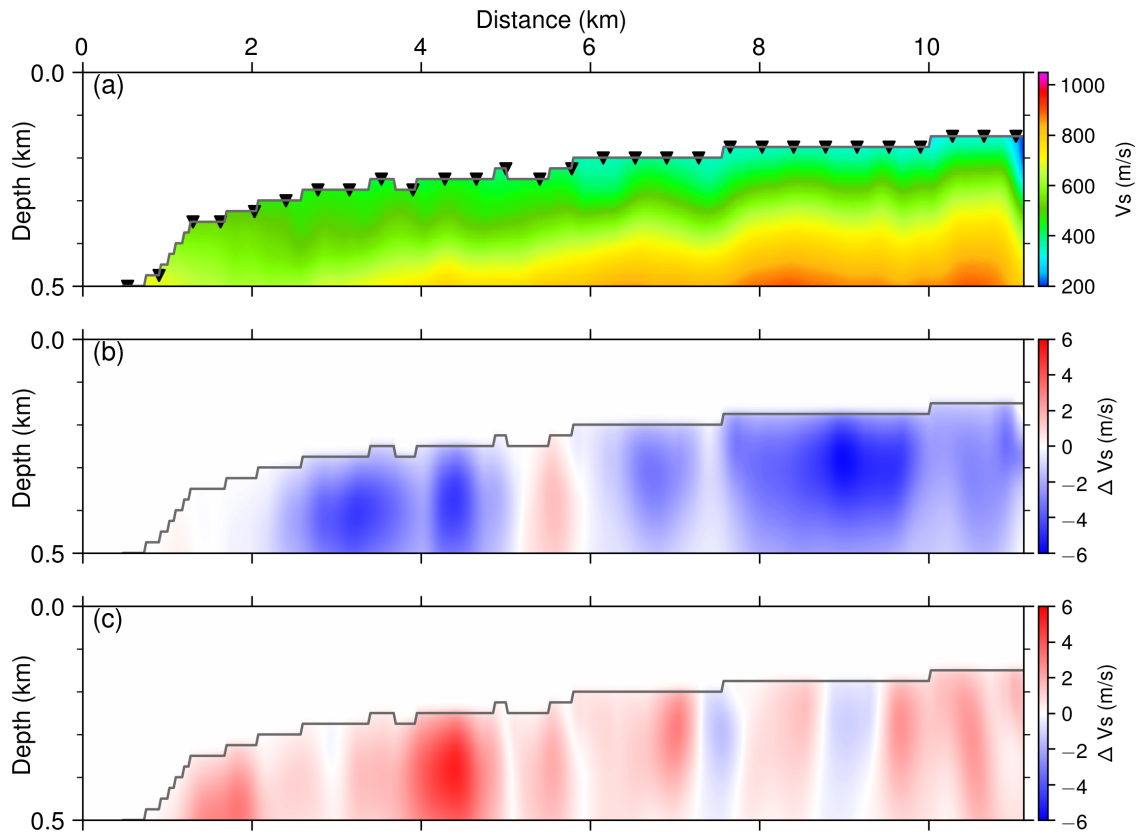


Figure S10. The same with Fig. S9 but for Line 4324 and the starting model for baseline FWI is Fig. S3c.

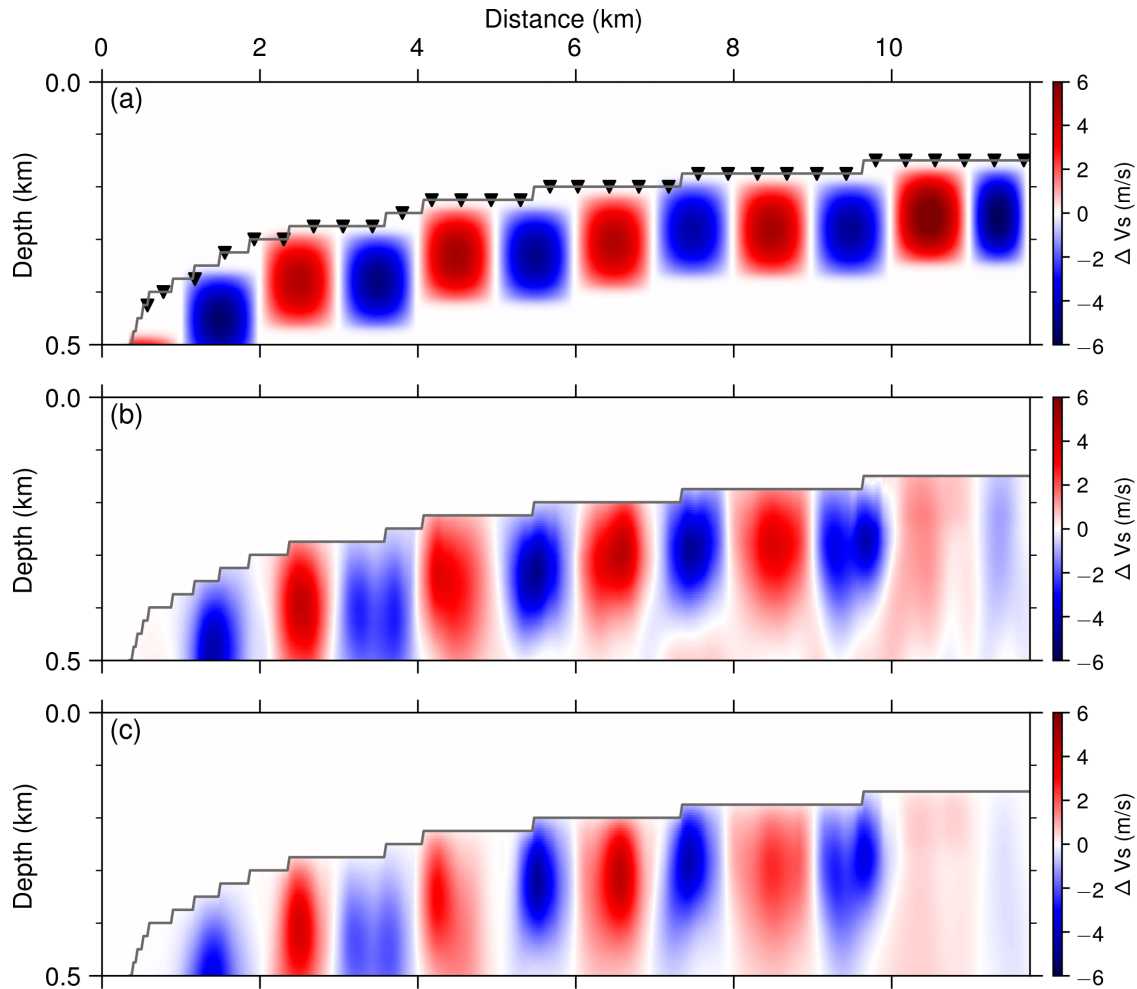


Figure S11. The 'true' time-lapse model was generated by adding 1% positive and negative Gaussian-shape velocity anomalies to the baseline velocity model (Fig. 4a). Each of the anomaly has 1 km lateral extension and 0.2 km thickness. The baseline data was generated using the baseline velocity model (Fig. 4a), and the monitoring data was generated using the 'true' time-lapse model. As a benchmark tests, DD-WI starts from the true baseline model (Fig. 4a) to see how well these perturbations can be recovered. (a) The true velocity anomalies (changes), (b) the inverted velocity anomalies from DD-WI using waveform differences, and (c) the inverted velocity anomalies from DD-WI using arrival time differences. The inverted velocity anomaly model is used as the benchmark for the following tests.

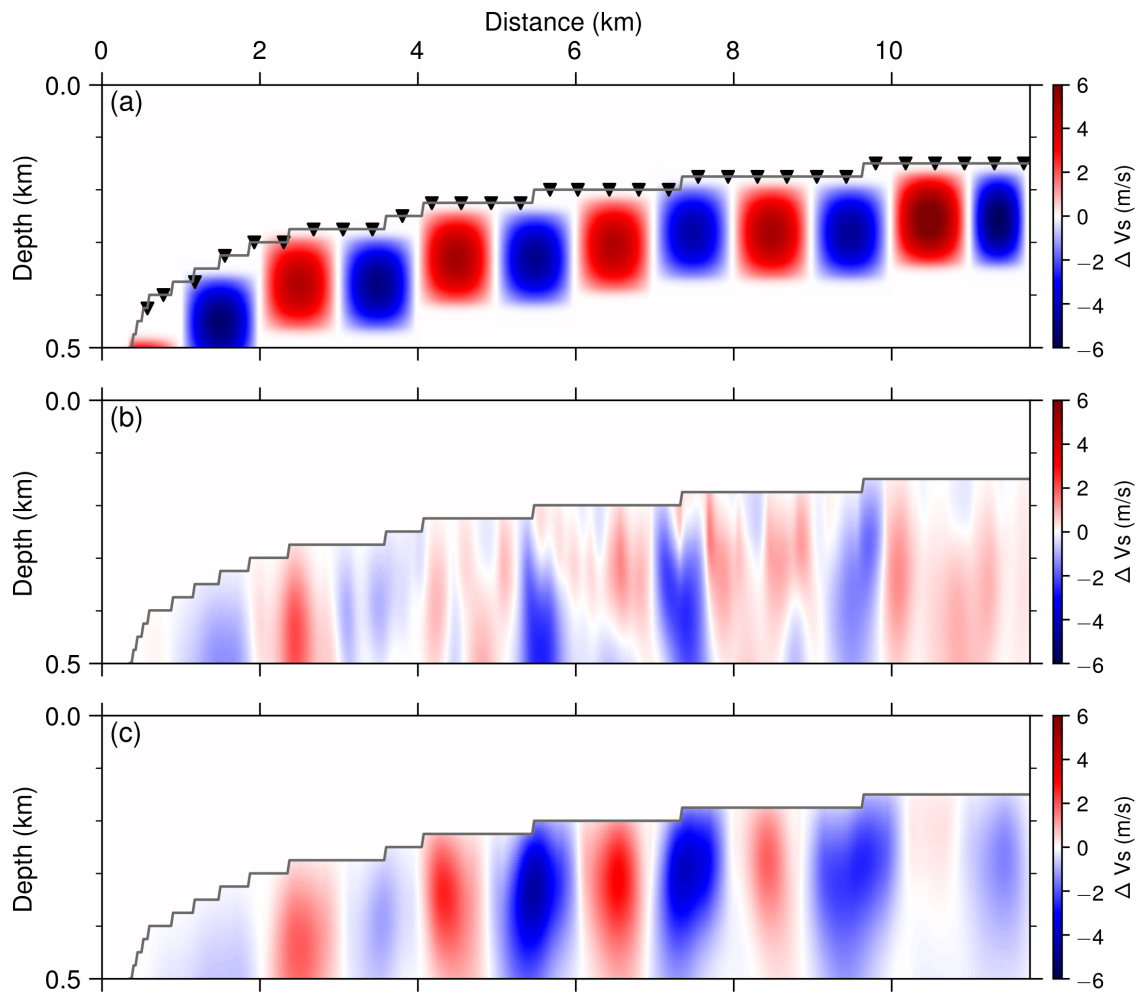


Figure S12. The same with Fig. S11, except that instead of starting DD-WI from the 'true' baseline model (Fig. 4a), we use the model in Fig. S3a as the starting model for DD-WI. The model difference between Fig. S3a and Fig. 4a are much larger than the added velocity anomalies. (a) The true velocity anomalies, (b) the inverted velocity anomalies from DD-WI using waveform differences, and (c) the inverted velocity anomalies from DD-WI using arrival time differences.

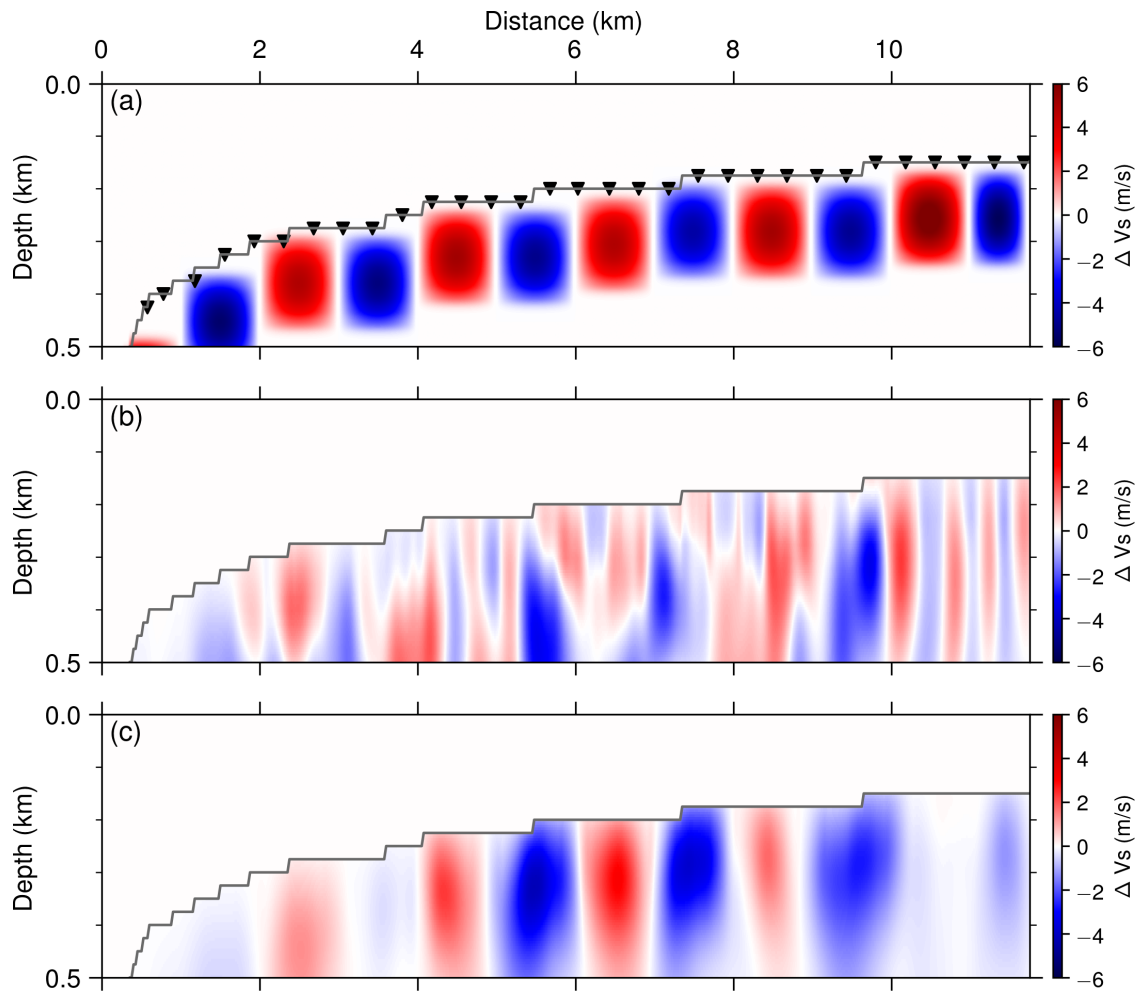


Figure S13. The same with Fig. 12, except that we add noise into the baseline and monitoring data. Signal to noise ratio (S/N) is about 8, lower than that of the extracted CC functions (Fig. 1c) from ambient noise. (a) The true velocity anomalies, (b) the inverted velocity anomalies from DD-WI using waveform differences, and (c) the inverted velocity anomalies from DD-WI using arrival time differences.

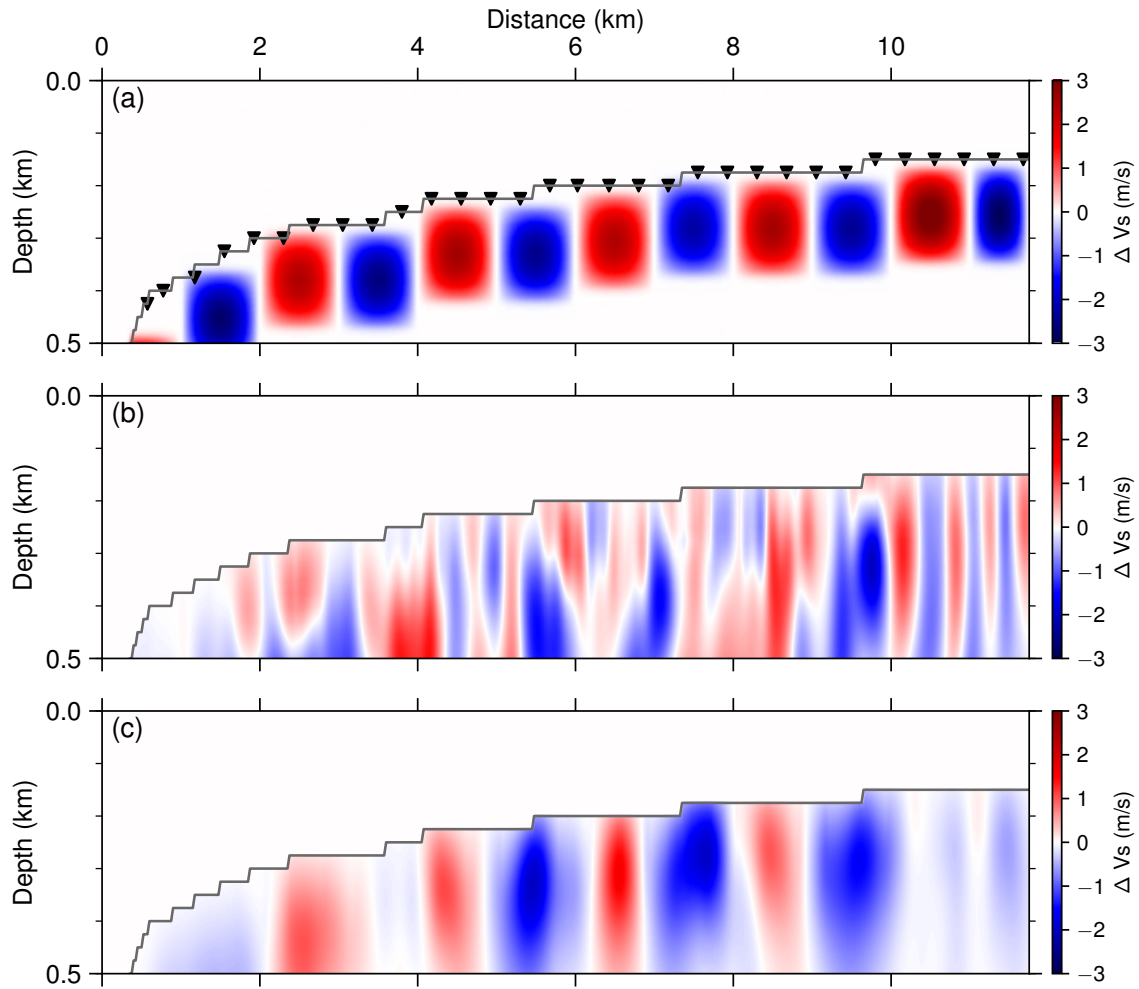


Figure S14. The same with Fig. 13, except that the added velocity anomalies are more subtle, 0.5% of the background velocity. (a) The true velocity anomalies, (b) the inverted velocity anomalies from DD-WI using waveform differences, and (c) the inverted velocity anomalies from DD-WI using arrival time differences.

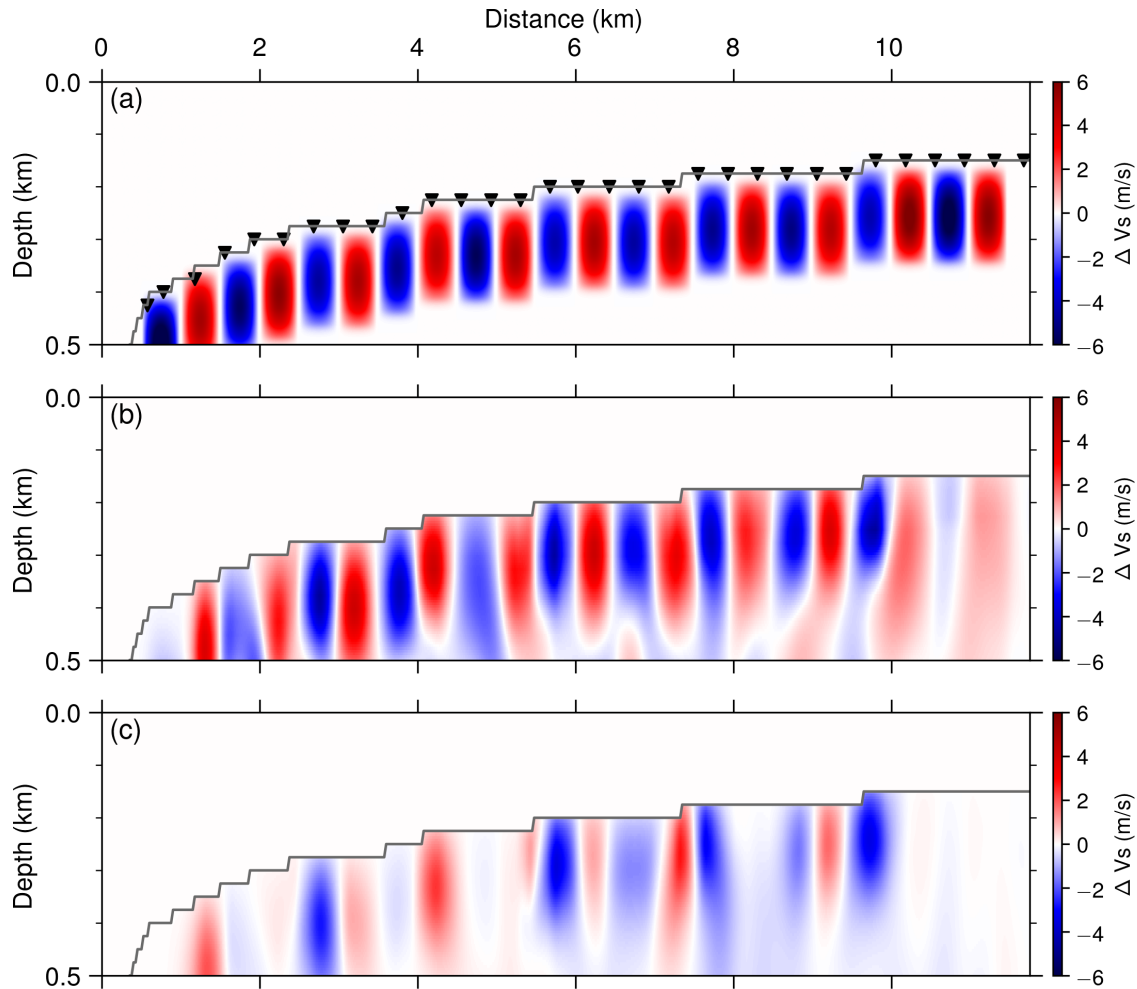


Figure S15. The 'true' time-lapse model was generated by adding 1% positive and negative Gaussian-shape velocity anomalies to the baseline velocity model (Fig. 4a). Each of the anomalies has 0.5 km lateral extension and 0.2 km thickness. The baseline data was generated using the baseline velocity model, and the monitoring data was generated using the 'true' time-lapse model. As a benchmark test, DD-WI starts from the true baseline model (Fig. 4a) to see how well these perturbations can be recovered. (a) The true velocity anomalies, (b) the inverted velocity anomalies from DD-WI using waveform differences, and (c) the inverted velocity anomalies from DD-WI using arrival time differences. The black triangles in (a) indicate the locations of OBNs. This test is used as the benchmark for Fig. S16.

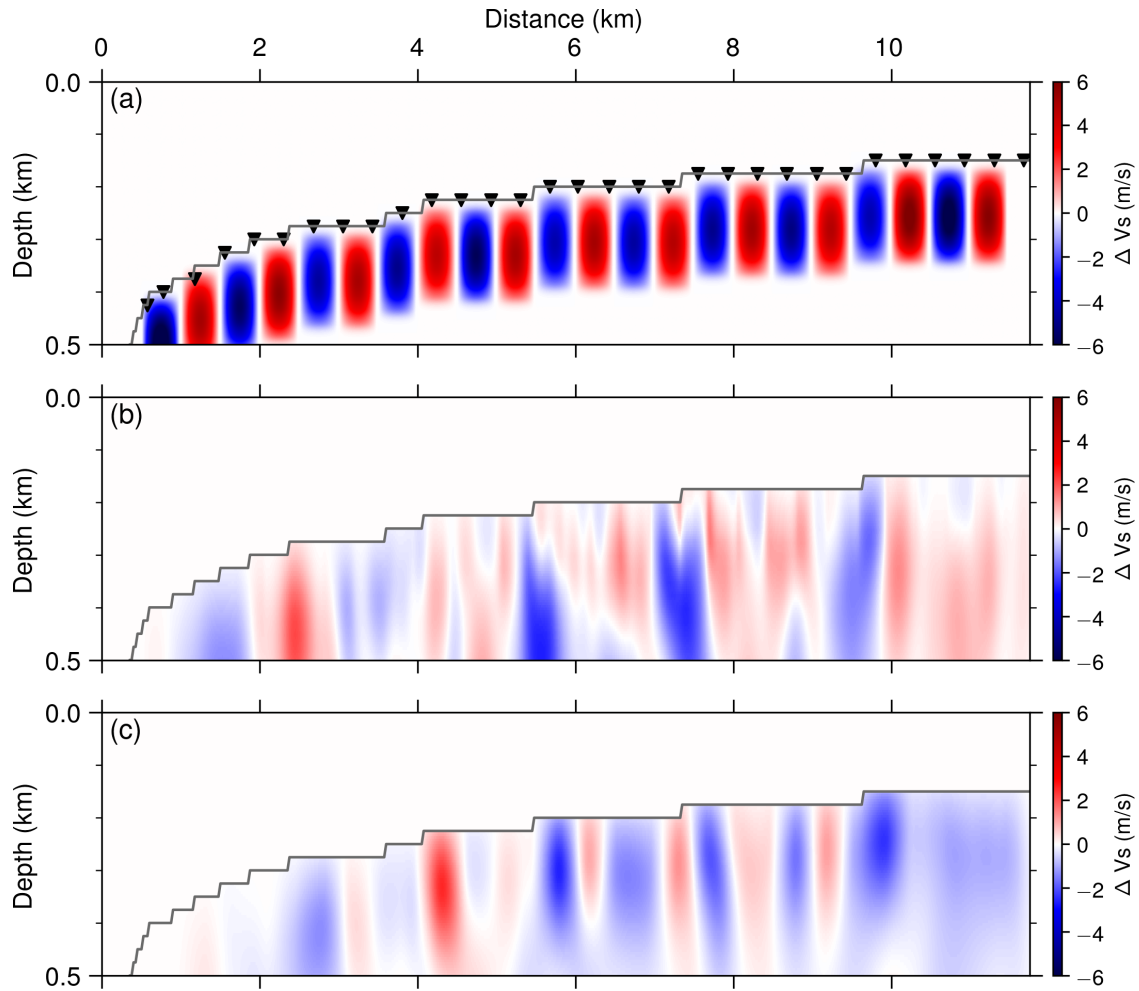


Figure S16. The same with Fig. S15, except that instead of starting DD-WI from the 'true' baseline model (Fig. 4a), we use the model in Fig. S3a as the starting model for DD-WI. The model difference between Fig. S3a and Fig. 4a are much larger than the added velocity anomalies. (a) The true velocity anomalies, (b) the inverted velocity anomalies from DD-WI using waveform differences, and (c) the inverted velocity anomalies from DD-WI using arrival time differences.